



A highly integrated shape memory alloy actuator and precision self-sensing tracking control based on position compensation

Ze Wang^{*}, Zihang Shang, Chuxiong Hu, Yu Zhu

State Key Lab of Tribology, Department of Mechanical Engineering, Tsinghua University, Beijing, 100084, China

Beijing Key Lab of Precision/Ultra-Precision Manufacture Equipment and Control, Tsinghua University, Beijing, 100084, China

ARTICLE INFO

Keywords:

Shape memory alloy wires
Actuator
Self-sensing
Tracking control
Position compensation

ABSTRACT

Shape memory alloy (SMA) actuators are widely used in various actuators due to their advantages of simplicity, high strength, and flexibility. The mapping relationship between the resistance change and displacement during the phase transition process of SMA enables its self-sensing control without external displacement sensors. However, the limited accuracy and high complexity of existing self-sensing models are two crucial factors restricting the wide application of self-sensing control. Due to the high nonlinearity of the SMA wire's phase transition process, it is challenging to achieve accurate position estimation using a simple self-sensing model. Thus, this paper proposes a novel approach by utilizing the simplest linear model for position estimation. The inevitable modeling errors are directly compensated in the final control results, rather than compensating for estimation errors. This significantly reduces the implementation difficulty of SMA self-sensing control and effectively improves control accuracy. Furthermore, a highly integrated prototype of SMA actuator is designed in this paper, where the additional position sensor and self-resetting loading device are integrated, greatly reducing the size of the SMA actuator. A series of self-sensing tracking experiments are conducted on this prototype, validating that the compensated self-sensing control can achieve comparable performance to the control method with external sensors.

1. Introduction

Electric actuators are important components in mechatronics systems. Conventional motors, as commonly understood, have reached a relatively mature stage and are widely used in various fields, such as CNC machine tools [1,2], precision motion platforms [3–5], and so on. However, in special scenarios that require fast response, miniaturization, flexible driving, and harsh operating conditions, conventional motors based on electromagnetic induction principle still have certain limitations. Therefore, special actuators composed of materials such as piezoelectric materials and dielectric elastomers have received widespread attention in recent years.

Shape memory alloys (SMA), under the influence of methods such as electrical heating, undergo reversible phase transformation and exhibit a certain degree of shape change, known as the shape memory effect. Based on this, SMA wires, with Ni-Ti alloy being a typical representative, can achieve displacement changes of approximately 5% of their total length under the action of relatively small currents and return to their original shape after the current is disconnected, making them possess the basic characteristics of an actuator. In addition, SMA wires typically have many unique advantages, such as high energy density, high flexibility, and biocompatibility [6]. They

have been widely applied in various fields, including robotics [7], artificial muscles [8], biofabrication [9], medical devices [10], and automotive applications [11]. Furthermore, SMA wires can also be used to drive grippers. In [12,13], a novel gripper structure driven by SMA wires was designed, characterized by utilizing very long SMA wires in conjunction with pulley systems and other transmission devices to achieve longer gripping motion. Many similar studies utilize clever structural designs to maximize the advantages of SMA wire actuators. Additionally, in [14], a planar soft actuator driven by SMA was introduced, and corresponding modeling and control work were conducted. The possibility of using SMA actuators as middle ear prosthesis and analysis of their dynamic and vibrational characteristics were investigated in [15]. [16] presented an exploration of the possibilities of using origami structures as SMA actuators, revealing more potential applications.

The above work has fully demonstrated that SMA can constitute various forms of actuators. However, due to the complexity of the phase transformation process, the contraction of SMA wires caused by phase transformation is also influenced by multiple factors. The relationship between displacement and the current applied to SMA wires often exhibits significant hysteresis nonlinearity, which severely

^{*} Corresponding author at: State Key Lab of Tribology, Department of Mechanical Engineering, Tsinghua University, Beijing, 100084, China.
E-mail address: wangze20@tsinghua.edu.cn (Z. Wang).

limits the improvement of control effectiveness. To address this issue, an improved phase transformation equation incorporating the Logistic function was proposed in [17] to further reduce the impact of noise and other disturbances during the phase transformation and displacement process. Similarly, [18] summarized a more comprehensive hysteresis model that includes additional factors such as load and temperature through extensive experiments, significantly enhancing the robustness of the control system for SMA actuators. In addition to more accurate models describing the phase transformation process, some intelligent control strategies have also been developed to improve control performance without relying on a specific model. For example, the fuzzy PID controller [19] can enhance the response speed of helical SMA actuators, reduce delays during tracking processes, and effectively prevent the problem of overheating of SMA wires caused by control saturation. Besides fuzzy PID, appropriate fuzzy neural networks [20] can also provide relatively accurate and fast descriptions of hysteresis phenomena without a clear physical model. Considering the controllability issue where the heating process of conventional SMA actuators is controllable while the cooling process is not, active cooling devices were incorporated into the design of SMA actuators in [21,22], which effectively improved the speed and controllability of the reverse displacement process of SMA wires.

Another outstanding performance of SMA wires as actuators is their ability to self-sense their deformation displacement without the need for additional measurement devices. The principle of self-sensing lies in the fact that not only does the displacement of SMA wires change during the phase transformation process, but their resistance also undergoes significant changes. By establishing a mapping relationship between resistance and displacement, the resistance of the SMA wire can be determined indirectly through the voltage and current in the circuit, thus indirectly measuring the displacement. This eliminates the need for dedicated displacement sensors for the actuator, effectively reducing the size of the actuator and maximizing the advantages of lightweight SMA actuators. In Ref. [23], the measurement signal of differential resistance was used to perceive displacement and achieve closed-loop control. In addition to linear displacement sensing, this method is also applicable to rotary motion mechanisms composed of dual SMA wires, and basic closed-loop control can still be achieved with sliding mode control [24]. However, there is obviously a significant nonlinearity in the relationship between resistance and displacement, which is even more complex than the nonlinear relationship between current and displacement. Therefore, improving the accuracy of this nonlinear self-sensing model becomes the focus of research on self-sensing control of SMA. Literature [25,26] constructed a model of resistance variation during the phase transformation process through a large number of experiments to achieve relatively robust position self-sensing estimation. However, this approach places high demands on the consistency of the SMA wire itself, and the difficulty of displacement calculation using complex models should not be ignored. In addition to theoretical models, it has been proven that RBF neural networks [27] and deep neural networks [28] can also obtain relatively accurate resistance–displacement self-sensing models. Recent studies have shown that machine learning methods can establish self-sensing models for force and stiffness as well, providing more choices for accurate multidimensional measurement solely based on the single information source of resistance [29]. However, the above neural network-based research does not consider the complexity and real-time performance of computation. Complex black box models, especially the computation process of deep neural networks, are not suitable for real-time feedback of SMA actuators. Moreover, the construction of neural networks requires extensive training with a large amount of pre-existing data, and the issues of performance consistency during the training process and their impact on the subsequent service life of SMA wires have not been thoroughly studied. From an application point of view, SMA actuators, especially those with self-sensing capabilities, can also be utilized for driving in confined spaces, such as the focusing

module in mobile phone cameras, thanks to their compact size and the advantage of not requiring additional installation of displacement sensors (According to Huawei's publicly disclosed patents, SMA wires have been effectively applied in smartphones due to their advantages such as small space requirement, high actuation force, and self-sensing control without sensors).

The above research work has fully demonstrated the broad application prospects of SMA actuators. Their unique self-sensing characteristics give them significant advantages in achieving high integration control. However, the displacement estimation accuracy of existing self-sensing models cannot meet the requirements of precision motion control for actuators. Due to the highly nonlinear nature of the phase transformation process, there is an inherent contradiction between improving modeling accuracy and reducing model complexity. This means that it is difficult to achieve accurate displacement estimation through simple models, while complex models often have difficulties in calculation and cannot meet the real-time requirements of feedback control. [30] describes the nonlinear change of position accurately during the phase transformation process of SMA by using a more precise self-sensing model, and improves the closed-loop tracking effect with a fuzzy logic controller. The idea of Ref. [31] is consistent with that of [30], and the main academic contribution is to improve the self-sensing model and control accuracy, as well as to apply it in SMA drivers in grippers. The idea of Ref. [25] is to select an appropriate SMA wire to make an actuator, effectively eliminating the influence of the R phase factor during the phase transformation process, reducing the degree of nonlinearity of the self-sensing model, and thus improving the self-sensing control effect.

To address the above issues of SMA self-sensing, this paper designs a highly integrated prototype of SMA actuator, which does not require additional laser measurement devices and has a more compact structural layout than other published literature. Based on this prototype, a precision self-sensing control strategy based on displacement compensation is proposed in this paper. It can effectively compensate for tracking errors in the self-sensing control process with a standard displacement sensor as a reference. This compensation strategy is different from conventional modeling compensation and adopts a novel approach of directly compensating trajectory tracking errors. It can effectively ensure the final trajectory tracking control performance even when the displacement estimation error of the self-sensing model is not accurate enough. The core contribution of this paper is not an accurate self-sensing model, but the compensation stage for position accuracy. We only use the simplest linear model to estimate the position of the moving element, which is simple enough to ensure the feasibility of self-sensing in real industrial applications. For inevitable position estimation errors, we propose a compensation method, which is proved to be effective in improving tracking control under modeling inaccuracies through both theoretical analysis and experiments. Therefore, this paper provides a completely different approach from the traditional SMA self-sensing control, focusing directly on the final tracking control effect rather than emphasizing the accuracy of the self-sensing model. This can effectively reduce the implementation difficulty of self-sensing control and is of great significance for its industrial applications. In addition, various types of trajectory tracking experiments have been conducted. The experiments on smooth trajectory tracking demonstrate that the proposed compensation scheme (in the absence of such sensors) can achieve similar tracking control performance to the case with external sensors.

2. Self-sensing SMA actuator

In order to further demonstrate the miniaturization and self-sensing capabilities of SMA wire, this paper proposes a novel prototype of the SMA actuator. Unlike other SMA actuators presented in other published papers, this proposed one does not require additional loading devices or laser measurement devices to achieve digital displacement control, making it highly integrated. Additionally, the self-sensing characteristics of the SMA wire in this prototype will be analyzed.

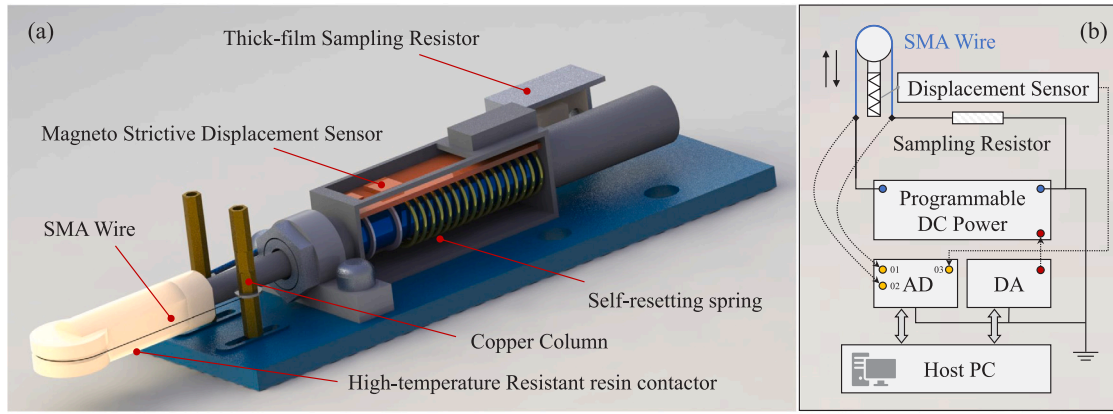


Fig. 1. (a) Design of the SMA actuator prototype. (b) Working principle.

2.1. Design of the highly integrated SMA actuator

The designed SMA actuator in this paper is shown in Fig. 1(a). The core driving component is a Ni-Ti SMA wire (manufactured by Suzhou Xinghai Co., Ltd.), which has a total length of 80 mm and a diameter of 0.15 mm. It operates under a load of 150 Mpa and within a temperature range of $-40\text{ }^{\circ}\text{C}$ to $80\text{ }^{\circ}\text{C}$. The theoretical service life is $\geq 200,000$ cycles, meeting the working condition requirements of general actuators. Both ends of the SMA wire are fixed on conductive copper columns on the bakelite substrate, passing through the contactor made of high-temperature-resistant resin (withstanding temperatures above $100\text{ }^{\circ}\text{C}$) fabricated via 3D printing. The contactor is connected to a self-resetting spring at the back end, continuously providing a preload force of 2.6 N to ensure that the SMA wire remains in a preloaded state. Additionally, the prototype includes a thick-film sampling resistor with a nominal resistance of $1\ \Omega$. It is connected in series with the SMA wire, and its resistance remains relatively constant regardless of current magnitude and temperature, facilitating auxiliary measurement of circuit current and resistance of SMA wire. Another clever design of this prototype is integrating a magnetic displacement sensor with analog output (0–10 V analog voltage linearly corresponding to 0–25 mm displacement with a resolution of $10\ \mu\text{m}$) within the chamber where the self-resetting spring is located. When the SMA wire drives the rigid linkage and spring for extension and contraction, the sensor can accurately measure the displacement changes of the contactor without increasing the size of the prototype.

The working principle of the prototype SMA actuator is shown in Fig. 1(b). Generally, the SMA wire undergoes a phase transformation from martensite to austenite by generating Joule heating when electrically heated. This transformation drives the contactor and the spring to produce a contraction displacement. Upon ceasing the electrical current, due to the characteristics of SMA, the reverse phase transformation from austenite to martensite occurs, causing the actuator to restore to its original position under the constant restoring force of the resetting spring. This process can be achieved by real-time control of the voltage across the series circuit composed of the SMA wire and the sampling resistor. Since the resistance of the SMA wire varies between $4\text{--}5\ \Omega$ and the resistance value of the sampling resistor (R_s) is fixed at $1\ \Omega$, the driving current is typically less than 500 mA. Therefore, the programmable DC power supply is set to have a voltage range of 0–3 V for its power input. The voltage of this DC power can be controlled by an external digital-to-analog converter (DA). Additionally, to accurately obtain the resistance of the SMA wire in real-time, the voltage drops across the sampling resistor (u_1), and the total voltage drop across the series circuit (u_2) are measured based on the grounded configuration shown in the figure. Consequently, the relationship between the resistance of the SMA wire R_{sma} and the sampling resistor R_s can be

expressed as follows:

$$R_{sma} = R_s \frac{u_2 - u_1}{u_1} \quad (1)$$

In addition, the displacement feedback values provided by the integrated displacement sensor can also be measured using an AD board. It should be noted that the negative terminals of the AD module, DA module, and DC power supply are all connected to the ground. Therefore, it is only necessary to measure and control the voltage at the positive terminal. The data collected by the AD module and the control commands from the DA module are monitored and controlled through a host computer. The physical diagram of the designed SMA actuator prototype is shown in Fig. 2. The AD and DA modules processing resolution of 16 bits are produced by RT-Links Co., Ltd. They work with a real-time sampling and control frequency of 5 kHz, which meets the requirement of the accuracy and speed of experimental data collection.

2.2. Analysis of self-sensing mechanism of SMA

To investigate the self-sensing characteristics of the designed SMA actuator, this section conducted tests on the SMA actuator under different heating and cooling processes. Firstly, five different heating cases, denoted as C1–C5, are provided. The corresponding variations of the series circuit voltage (u_2) are shown in Fig. 3(a). To avoid the issue of inaccurate resistance measurement caused by extremely low circuit currents, the minimum voltage during the testing process is set to 0.1 V. In C1, the voltage uniformly increases from 0.1 V to 2.6 V over a period of 50 s. Methods C2 and C3 have voltage increase rates that are twice (25 s) and four times (12.5 s) that of C1, respectively. In C4, the voltage starts at 0.1 V and increments by 0.5 V every 10 s. In C5, the voltage linearly increases from 0.9 V to 1.8 V. It should be noted that the measured values of the circuit voltage shown in Fig. 3(a) exhibit certain deviations from the set values mentioned above.

Fig. 3(b) depicts the displacement variations (measured by the displacement sensor) corresponding to the aforementioned five heating processes. From the figure, the following observations can be made:

1. Under the same voltage but different heating processes, the displacements of the SMA are nearly identical.
2. The displacement rate is positively correlated with the voltage increase rate. Between 1 V and 2 V, the displacement is most sensitive to voltage changes.
3. The displacement trends of C5 and C1 are similar, indicating that the initial voltage does not significantly affect the displacement variation of the SMA.

Based on these observations, it can be preliminarily concluded that the displacement of the SMA wire exhibits good consistency during the heating process.

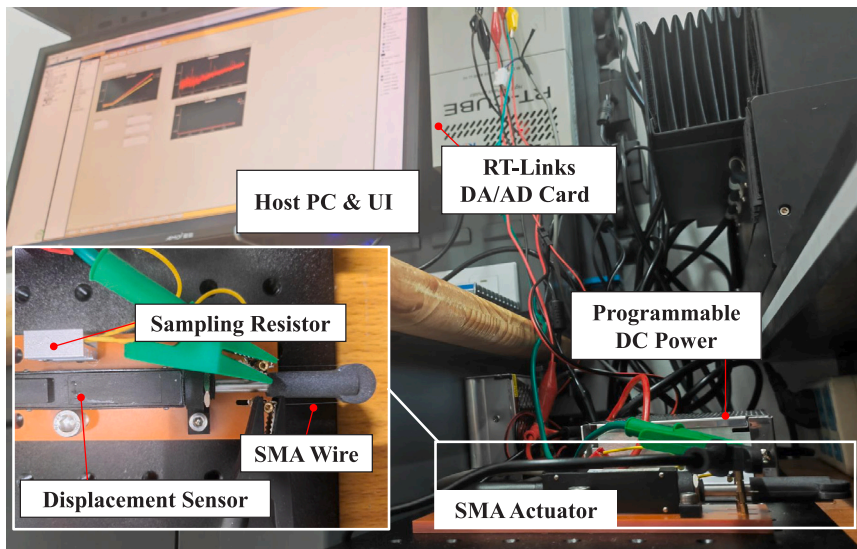


Fig. 2. The prototype of SMA actuator.

Additionally, Fig. 3(c) presents the corresponding resistance of the SMA wire, showing a similar consistency as the displacement. It should be noted that the resistance fluctuates more noticeably in the low-voltage range compared to the high-voltage range. This is because the signal-to-noise ratio is lower at low voltages, which poses a challenge in mitigating the effects of measurement noise in subsequent controller design.

Finally, the relationships between the resistance of the SMA wire and the corresponding displacement are illustrated in Fig. 3(d), which is crucial for achieving self-sensing measurements. Overall, the relationship between the two is nonlinear, determined by the characteristics of different phases during the phase transition. However, based on the results shown in the figure, it can be observed that the relationship approximates linearity when the displacement is between 5.2 mm and 5.7 mm. Additionally, it is pleasing to note that the resistance–displacement curves for the five different heating methods (C1–C5) overlap, which is an essential prerequisite for approximately estimating the displacement of the SMA wire using resistance in diverse application scenarios. It should be noted that since Fig. 3 only presents the heating process, it does not constitute a common hysteresis loop.

It should be noted that, The displacement shown in Fig. 3 and other figures involving displacement refers to the displacement relative to the zero point of the integrated displacement measurement sensor in the actuator. In order to ensure effective initial loading on the SMA wire in the designed prototype, the extension value of the constant force spring must match the length of the SMA wire. This inevitably results in a non-zero displacement measurement value for the SMA wire when it is not energized (initial state). However, since the displacement measurement results and zero point definition are relative, if we define the displacement in the initial state as the zero point, we can ensure that the initial displacement at $t = 0$ is zero, without affecting the final tracking error results. In the revised version of the paper, we still adopt the previous approach, as under different loads, readers may question whether there will be initial position offsets. Defining the zero point as the displacement at $t = 0$ is not sufficiently persuasive.

To further analyze the self-sensing characteristics of the SMA wire comprehensively, similar cooling experiments, i.e., C6–C10 are performed, and the results are shown in Fig. 4. From Fig. 4(a), it can be observed that the three cases, C6–C8, can be considered as the reverse cooling processes corresponding to C1–C3 (voltage decreasing from 2.6 V to 0.1 V). In case C9, the voltage uniformly decreases from 1.7 V to 1.2 V within 1 s and remains constant, while in case C10, the voltage decreases from 1.5 V to 0.5 V over 20 s. The displacement

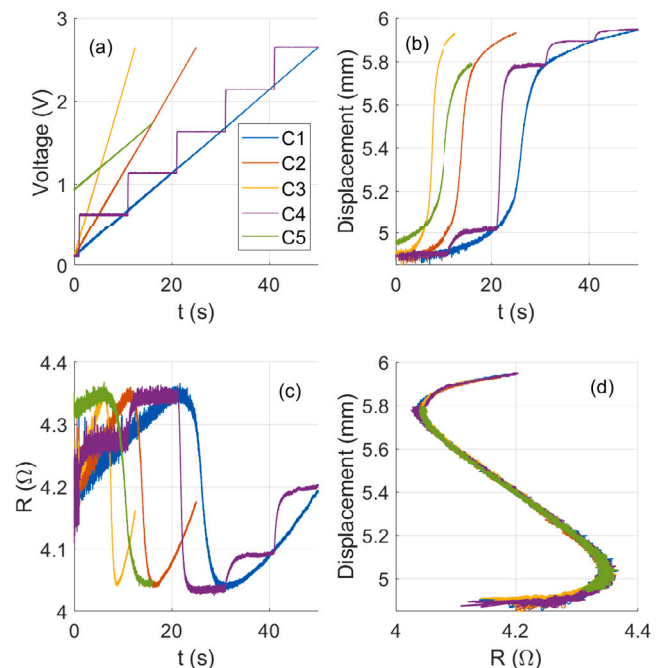


Fig. 3. SMA wire characteristics during different heating processes: (a) Voltage of the series loop. (b) Measured displacement. (c) resistance of the SMA wire R_{sma} . (d) Relationship between R_{sma} and displacement.

and resistance variations of the SMA wire during the above processes are plotted in Fig. 4(b) and (c), respectively. In contrast to the consistency shown in the heating process, the changes in resistance and displacement during the cooling process do not completely align with the voltage variations. In Fig. 4(a), the three curves of C8, C9, and C10 intersect at one point. However, at that moment, there are significant deviations in the corresponding displacement and resistance values among the three cases. This phenomenon is more pronounced in the resistance–displacement curve shown in Fig. 4(d). Even when lowering the voltage at the same rate under different initial voltages, it is still impossible to maintain a consistent relationship between resistance and displacement. This implies that, unlike the heating process, it is difficult to describe the relationship between displacement and resistance with a

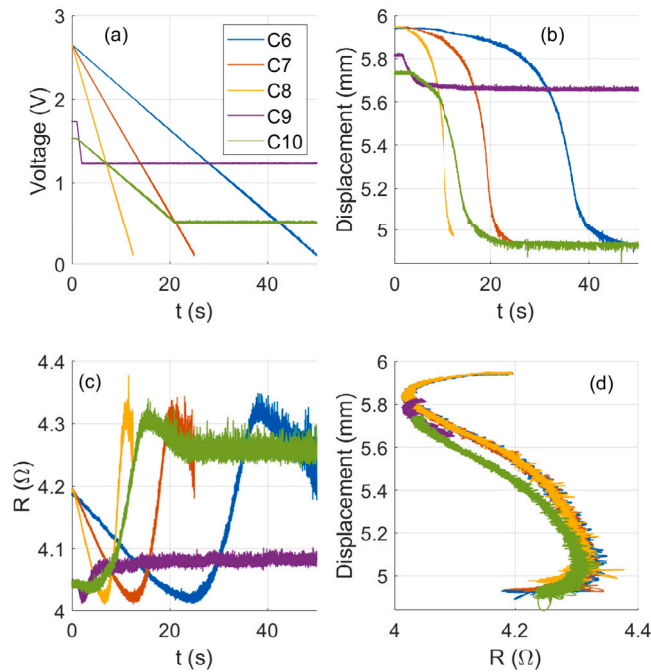


Fig. 4. SMA wire characteristics during different cooling processes: (a) Voltage of the series loop. (b) Measured displacement. (c) resistance of the SMA wire R_{sma} . (d) Relationship between R_{sma} and displacement.

relatively universal function during the cooling process. Undoubtedly, this poses certain challenges to self-sensing measurements.

In order to address this issue, previous studies have attempted to accurately describe this phenomenon through complex mathematical models or neural network models. However, the multivariable nonlinear modeling process involved is undeniably complex, which significantly limits the application of self-sensing methods in scenarios with strong real-time requirements such as tracking control. In the next section of this paper, a novel approach to linear modeling and compensation will be introduced, aiming to achieve high-precision self-sensing control without increasing the complexity of the model.

Since the SMA actuator in this paper uses an integrated position measurement sensor, the question of whether the subsequent self-sensing method is auxiliary sensing is explained as follows

- A small sensor for position sensing is indeed integrated into the actuator, but as emphasized in the paper, the function of this sensor is only to verify the accuracy of self-sensing and to conduct comparative tests under sensor-based conditions. Compared with the commonly used laser ranging method in other papers, this integrated installation method makes the actuator more compact.
- The measured data of the position sensor is indeed used in the compensation algorithm in this paper, but it should be noted that this data is not equivalent to real-time feedback measurement, but rather measures the actual tracking error for a specific tracking control task and calculates the compensation amount offline. Once the compensation amount is calculated offline, no sensor is needed anymore. This process can be regarded as calibration and compensation using real position measurement results, which is completely different from sensor-based control. The load test experiments listed in the paper are good proof because they use the same tracking trajectory as the no-load condition, so the compensation amount does not need to be recalculated, and only the compensation results of the no-load condition are used. In addition, for commonly used repetitive trajectory tracking tasks in industrial applications, no external displacement sensor information is required after completing one compensation amount calculation.

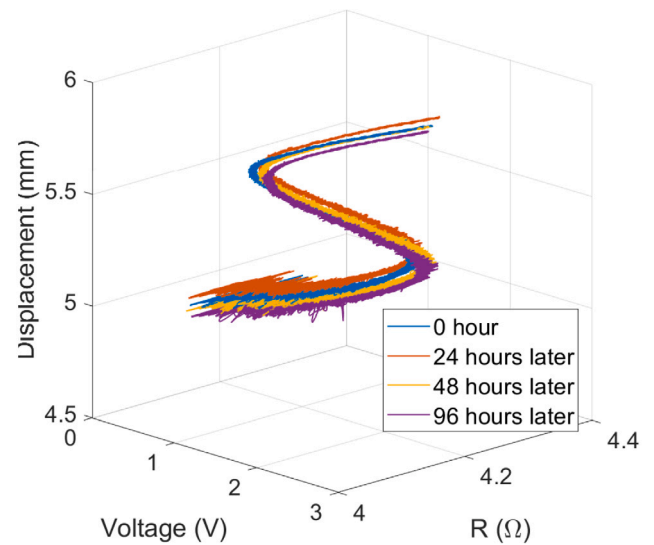


Fig. 5. The experimental results of heating tests performed at different time. (For interpretation of the references to color in this figure legend, the reader is referred to the web version of this article.)

2.3. Time invariance test of SMA self-sensing

The aforementioned experiments demonstrate the good self-sensing characteristics of the designed SMA actuator during the heating phase. However, for an actuator, maintaining consistent characteristics over long time periods is a fundamental requirement. In order to further confirm the potential for further application of the proposed SMA actuator, its self-sensing characteristics are tested over a long period of 96 h, and the experimental results are shown in Fig. 5. This 3D graph depicts the relationship between voltage, resistance, and displacement in four consecutive heating experiments conducted within the 96-hour period. The blue curve corresponds to the aforementioned Case C1, while the remaining curves represent the results obtained from repeating the same experiment as C1 after 24, 48, and 96 h. From the experimental results, it can be observed that the curves mostly overlap, and there is no significant change in the correspondence between voltage, resistance, and displacement. Although there are slight differences in the results of each experiment, they are mainly caused by the initial displacement deviation. We believe that this displacement deviation is primarily caused by the deviation generated in the copper column of the designed actuator prototype under the long-term thrust of the self-resetting spring. We believe that by further fixing the copper column and the substrate, this deviation can be effectively avoided. Additionally, this deviation is essentially a static deviation that is commonly present in mechanical actuation devices and can be effectively mitigated through calibration and other means. Therefore, we conclude that the designed SMA actuator and its self-sensing characteristics exhibit good time invariance over longer periods, indicating great potential for widespread industrial applications.

2.4. Variable load test of SMA self-sensing

In order to test the self-sensing characteristics under different loads we have changed the orientation of the actuator from horizontal to vertical, as shown in Fig. 6, and conducted comparative experiments without load, with additional loads of 10 g, 20 g, 30 g, and 50 g, respectively. We present the characteristic curves under different loads, with a constant voltage increase (same as C1), in Fig. 7. It can be observed that with the addition of load, there are slight variations in displacement and resistance during the transition phase during the

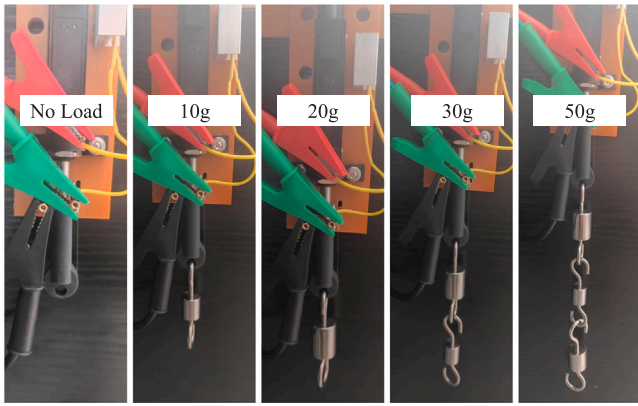


Fig. 6. SMA actuator with different loads.

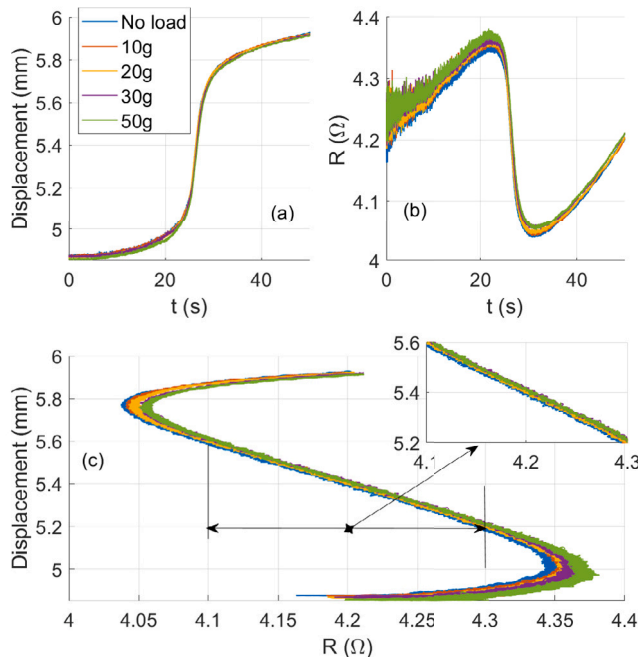


Fig. 7. SMA wire characteristics during heating processes with different loads: (a) Measured displacement. (b) resistance of the SMA wire R_{sma} . (c) Relationship between R_{sma} and displacement.

phase change, but the impact on the linear segment is minimal. Especially in the displacement-resistance coordinate graph, the test curves under different loads practically overlap in the linear segment. This strongly confirms the effectiveness of the proposed self-sensing model, which remains valid even under different external loads. In addition, we conducted cooling process tests, as shown in Fig. 8, and it can be observed that the influence of load on self-sensing characteristics is even smaller during the cooling process. The sets of characteristic curves under different loads practically overlap, maintaining a high level of consistency even during the transition process. Therefore, we have reason to believe that the variations in load that may occur in practical applications will not significantly affect the accuracy of the self-sensing model and control method proposed in this paper.

3. Self-sensing model and controller design

In this section, the self-sensing characteristics of the designed SMA actuator are further analyzed and modeled, and a control strategy

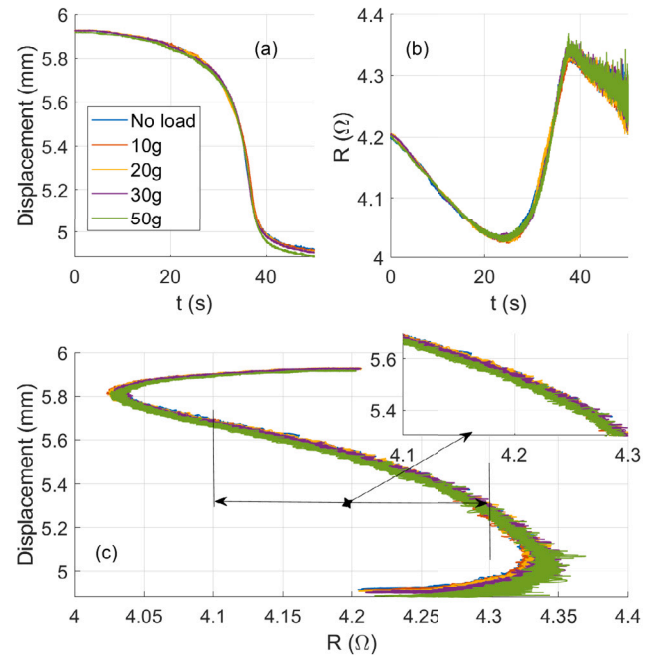


Fig. 8. SMA wire characteristics during cooling processes with different loads: (a) Measured displacement. (b) resistance of the SMA wire R_{sma} . (c) Relationship between R_{sma} and displacement.

using the self-sensing characteristics is designed to achieve accurate trajectory tracking and positioning.

3.1. Linear estimated model of displacement

In order to minimize the influence of measurement noise and other factors on modeling, we first applied zero-phase low-pass filtering to the resistance measurements and displacement measurements in C1–C10 separately. A 4th-order Butterworth low-pass filter with a cutoff frequency of 10 Hz was used as the filter. The filtered relationship between resistance and displacement is shown in Fig. 9. From the graph, it can be observed that the curves representing C1–C5 overlap, and together with the cooling process curves C6–C10, they form the hysteresis loop. Although there are significant differences between the resistance–displacement curves during the cooling and heating processes, the characteristics of C9 and C10 are closer to those of the heating process. This indicates that when the voltage decrease is small and within the middle part of working voltage range, the self-sensing characteristics of the heating process can be approximated. However, even so, due to the relative simplicity of the self-sensing model, there will inevitably be some estimation errors during the reciprocating displacement increase–decrease process. In our research work, we have taken a different approach, no longer pursuing absolute accuracy in modeling but aiming to improve positioning accuracy under self-sensing control through compensation methods.

To further simplify the self-sensing model, the effective working displacement of the SMA actuator is set to be between 5.1 mm and 5.7 mm. From Fig. 9, it can be observed that the relationship between displacement and resistance within this range can be approximately linear. By performing linear fitting on the filtered displacement (5.1 mm–5.7 mm) of the Case C1 and its corresponding filtered resistance data, the following self-sensing model can be obtained to describe the relationship between the estimated displacement and the resistance within the linear range:

$$S_e = kR_{sma} + b \quad (2)$$

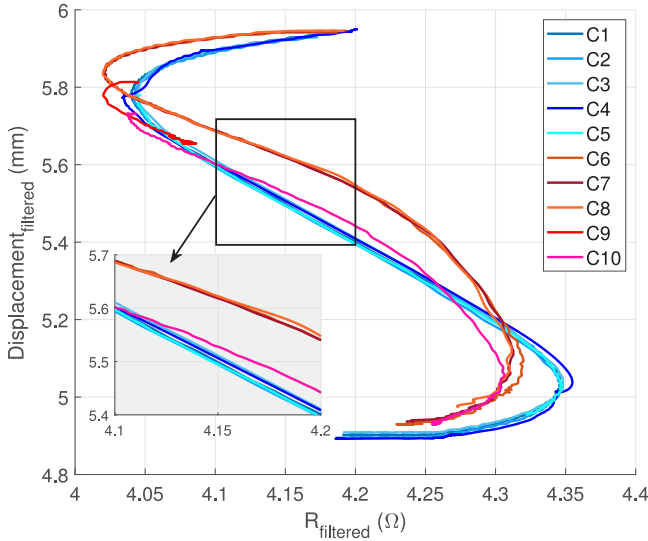


Fig. 9. Relationship between filtered R_{sma} and filtered displacement.

where S_e represents the estimated displacement, R_{sma} represents the measure resistance, and $k = -2.079$ and $b = 14.096$ are the slope and intercept of the linear fitting, respectively.

We take the C1 process as an example and plot the measured values, filtered results, and linear fitting results that describe the self-sensing characteristics in Fig. 10(a). From the figure, it can be observed that the fitting results calculated based on Eq. (2) are in good agreement with the measured values and filtered results. Additionally, Fig. 10(b) presents the measurement noise, which is the deviation between the displacement measurement and the filtered result. As can be seen from Fig. 10(b), there is a clear increase in measurement noise in areas where the resistance is too high or too low. This is primarily due to the transitional phase of SMA wire phase transformation corresponding to regions of excessively high or low resistance. During this phase, there is a significant nonlinearity between the displacement of the SMA wire and its resistance. The accumulation of these nonlinear characteristics, combined with inherent measurement noise, leads to a pronounced amplification of the measurement noise observed in Fig. 10(b) when the resistance is either too high or too low. Fig. 10(c) shows the estimation error, which is the deviation between the measurement values and the fitted estimated values. Through calculations, it is found that the root mean square (RMS) value of the measurement noise is $2.904 \mu\text{m}$, while the RMS value of the estimation error is $8.548 \mu\text{m}$. This value is smaller than the measurement resolution of the displacement sensor, i.e., $10 \mu\text{m}$, indicating its approximate accuracy to some extent.

Furthermore, from Fig. 10(c), it is evident that the estimation error has a certain regularity with respect to the resistance variation. If further nonlinear fitting is performed and compensated into the linear model of Eq. (2), the estimation accuracy will definitely be further improved. However, this study did not continue this work but instead looks forward to improving the final tracking and positioning accuracy through compensation strategies discussed in the following subsections, considering the insufficient accuracy of the model.

3.2. Closed-loop tracking controller and displacement compensation

In order to achieve precise tracking control using the simple self-sensing model described above, this paper designs a controller and corresponding compensation scheme as shown in Fig. 11. As mentioned above, during the motion of the SMA actuator, two position feedbacks are obtained: S_m , i.e., the actual measurement result obtained by the position sensor, and S_e , i.e., the result estimated based on the self-sensing characteristics using the resistance value. The designed control

scheme takes S_e as the feedback value, compares it with the desired command r , and a reasonable PID controller is designed to form a complete control loop. Due to the use of a simple linear self-sensing model, there will inevitably be a deviation between S_e and the measured value S_m . Therefore, even with excellent controller performance, it is difficult to achieve high tracking accuracy. Therefore, we further utilize the advantages of dual sensing and use the compensation of $e_m = r - s_m$ to compensate the control system for trajectory.

Similar to other common mechatronics systems, under the operation of a linear PID closed-loop controller, the displacement output of the SMA actuator at the time $n + 1$ depends on the state at time n and the input command. Based on this, the following state space representation can be obtained,

$$s_e(n+1) = vs_e(n) + \gamma r(n) \quad (3)$$

where v and γ represent linear gains, which characterize the relationship between the future motion state and the current state, as well as the system input. Assuming there are N sampling periods in a trajectory tracking control task, the control system of the designed SMA actuator can be represented by a state space model in the form of an lifted matrix, i.e.,

$$\mathbf{s}_e = \mathbf{G}\mathbf{R} + \mathbf{D} \quad (4)$$

where $\mathbf{s}_e = [s_e(0), s_e(1), \dots, s_e(N-1)]^T$, $\mathbf{R} = [r(0), r(1), \dots, r(N-1)]^T$, $\mathbf{D} = [s_e(0), s_e(0)v, \dots, s_e(0)v^{(N-1)}]^T$, and

$$\mathbf{G} = \begin{bmatrix} 0 & 0 & 0 & \dots & 0 \\ \gamma & 0 & 0 & \dots & 0 \\ v\gamma & \gamma & 0 & \dots & 0 \\ \vdots & \vdots & \vdots & \ddots & \vdots \\ v^{N-2}\gamma & v^{N-3}\gamma & v^{N-4}\gamma & \dots & 0 \end{bmatrix}$$

The actual tracking error sequence without compensation can be represented as follows,

$$\mathbf{E}_m = \mathbf{R} - \mathbf{S}_m = [e_m(0), e_m(1), \dots, e_m(N-1)]^T \quad (5)$$

As shown in Fig. 11, the compensation term is added to the system as a kind of trajectory modification, and the specific compensation is designed according to the following steps:

Step 1: To suppress the high-frequency noise, the component of tracking error sequence is filtered by the low-pass filter Q . Thus the filtered results can be expressed by:

$$\mathbf{Y}_1(n) = \mathbf{E}_m * \mathbf{Q}_k(n), n = 0, 1, \dots, N-1 \quad (6)$$

where $*$ means the convolution operation, $\mathbf{Q}_k(n)$ is the impulse response of the filter Q , and \mathbf{Y}_1 is the temporary sequence.

Step 2: Inverse the filtered sequence \mathbf{Y}_1 , i.e.,

$$\mathbf{Y}_2(n) = \mathbf{Y}_1(N-1-n), n = 0, 1, \dots, N-1 \quad (7)$$

Step 3: \mathbf{Y}_2 is also filtered by the filter Q , i.e.,

$$\mathbf{Y}_3(n) = \mathbf{Y}_2(n) * \mathbf{Q}_k(n), n = 0, 1, \dots, N-1 \quad (8)$$

Step 4: Inverse the filtered sequence \mathbf{Y}_3 , i.e.,

$$\mathbf{Y}_4(n) = \mathbf{Y}_3(N-1-n) = \mathbf{E}_m * \mathbf{Q}_k(n) * \mathbf{Q}_k(N-1-N), n = 0, 1, \dots, N-1 \quad (9)$$

According to the property of convolution operation, there is no phase difference between \mathbf{Y}_4 and \mathbf{E}_m . Therefore one can obtain

$$\mathbf{Y}_4(n) = \Lambda(n)\mathbf{E}_m, n = 0, 1, \dots, N-1 \quad (10)$$

where $0 < \Lambda(n) < 1$ is the attenuation gain. Add \mathbf{Y}_4 into original \mathbf{R} as a kind of reference compensation, one can obtain the \mathbf{s}_e sequence after compensation, i.e., \mathbf{S}_{ec} according to Eq. (4).

$$\mathbf{S}_{ec} = \mathbf{S}_e + \mathbf{G}\Lambda\mathbf{E}_m \quad (11)$$

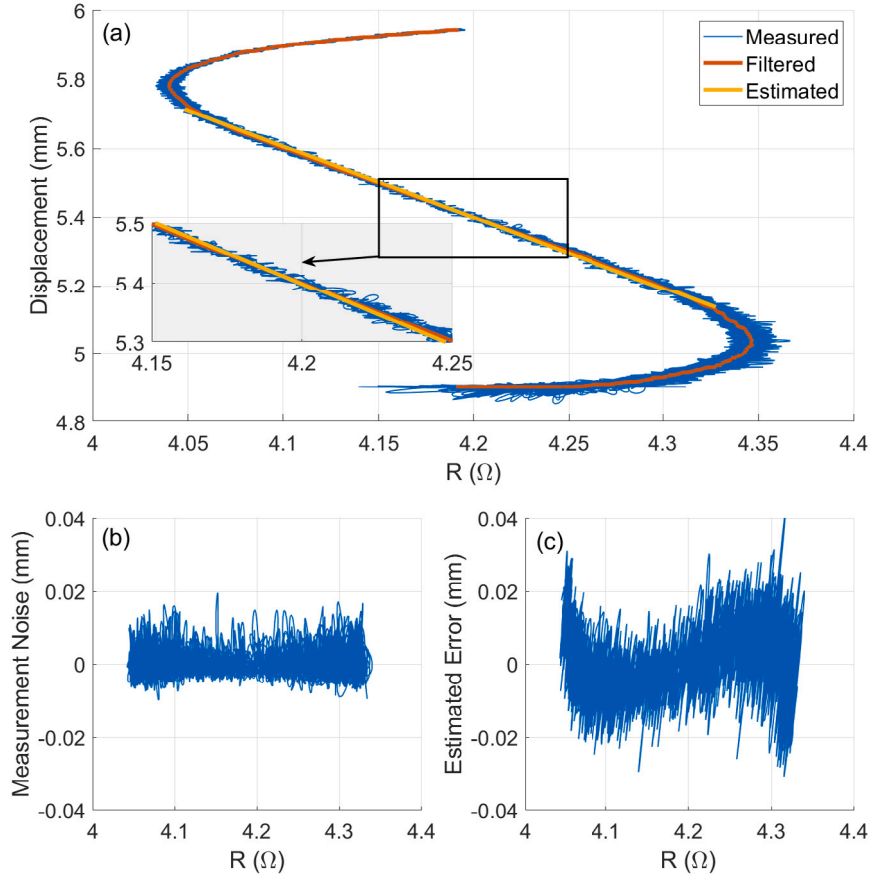


Fig. 10. (a) The estimated results of linear fit model. (b) Measurement noise. (c) Estimated error of the fit model.

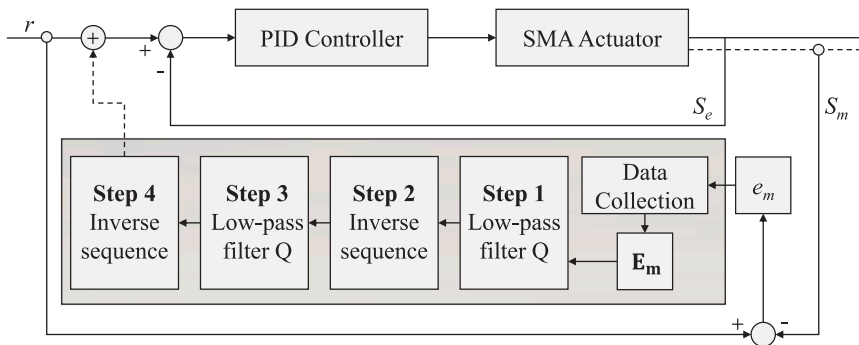


Fig. 11. Block diagram of the controller design.

Assuming that in each identical control task, the deviations between the two displacement feedbacks, i.e., S_e and S_m , are consistent, the compensated measured displacement S_{mc} and corresponding error sequence E_{mc} can be expressed by the following form:

$$S_{mc} = S_m + GA E_m \quad (12)$$

$$E_{mc} = (I - GA) E_m \quad (13)$$

It is clear that $\|I - GA\| < 1$, and the convergency of the proposed zero-phase error compensation scheme can thus be guaranteed.

4. Tracking control experiments and discussion

4.1. Experimental setup

To analyze the effectiveness of the aforementioned self-sensing model and compensation control strategy for SMA, different trajectory tracking experiments were conducted using the designed prototype of the SMA actuator in this section. The performance of the following three different types of control methods is compared:

Case I—With Sensor : The displacement sensor built into the prototype is used as position feedback, and a PID controller was employed for

Table 1
Estimated error of self-sensing.

	Square wave e_{rms}/e_{max} (μm)	Triangular wave e_{rms}/e_{max} (μm)	Sine wave e_{rms}/e_{max} (μm)	Sine wave (30 g) e_{rms}/e_{max} (μm)	Sine wave (50 g) e_{rms}/e_{max} (μm)
With sensor	21.78/198.57	19.02/104.39	11.02/42.05	12.29/45.18	14.75/57.39
Self sensing	15.64/103.03	18.17/73.38	13.90/54.02	13.15/45.46	12.52/39.16
Compensation	18.96/104.62	18.45/83.59	10.47/52.77	16.57/58.92	14.09/45.48

Table 2
Tracking performance of different trajectories.

	Square wave e_{rms}/e_{max} (μm)	Triangular wave e_{rms}/e_{max} (μm)	Sine wave e_{rms}/e_{max} (μm)	Sine wave (30 g) e_{rms}/e_{max} (μm)	Sine wave (50 g) e_{rms}/e_{max} (μm)
With sensor	11.28/315.51	13.49/37.57	5.99/19.50	5.50/19.29	5.51/21.45
Self sensing	17.86/318.45	42.88/78.77	14.77/44.49	12.44/35.94	11.66/29.75
Compensation	13.84/315.37	16.79/60.16	6.05/21.41	6.67/18.21	6.31/25.18

closed-loop control. The specific control parameters are set as $k_p = 30$, $k_i = 12$, $k_d = 0.6$.

Case II—Self Sensing : The estimated displacement obtained from the self-sensing model described in the previous sections is used as real-time feedback for closed-loop control. The controller was also a PID controller, and the control parameters are exactly the same as those in Case I.

Case III—Compensation : Zero-phase trajectory compensation, as mentioned earlier, is further added based on Case II.

The self-sensing estimation error and tracking error of the above three methods are analyzed for square wave, triangular wave, and sine wave trajectories. Tables 1 and 2 present the root mean square value (e_{rms}) and maximum absolute value (e_{max}) of the errors under different conditions, respectively. The estimated errors presented in Table 1 are the deviations between the proposed self-sensing model and the actual measurement results in this study. In Case I, II, and III, the estimated errors can be calculated based on the estimation results from the linear model and the measured positions. It is important to note that in Case I, the control process is achieved through sensor measurements for feedback, without utilizing the linear self-sensing model. The inclusion of estimated errors in different cases in this study aims to verify the accuracy of the self-sensing model under different conditions, i.e., whether the self-sensing model is used in the feedback loop. This is because utilizing the self-perception model in the feedback loop significantly affects the actual control performance, and different motion effects can also impact the accuracy of the proposed self-sensing model. Therefore, we provide estimated errors separately for different cases to account for these variations.

4.2. Tracking precision comparison results

First, we conducted a standard square wave trajectory tracking experiment. The square wave trajectory is shown in Fig. 12(a), with an amplitude of 0.3 mm and a period of 10 s. Fig. 12(b) shows the actual control results of three different cases. It is important to note that the plotted data is derived from the measurement values of the displacement sensor, rather than estimated one, so it can be considered as actual displacement data. The estimation error of the self-sensing characteristics and the actual tracking control error are plotted in Fig. 12(c) and (d), respectively. From Fig. 12(c), it can be observed that the estimated error increases due to the step change of the reference trajectory, especially at the moment of the trajectory's descent. This is because there is a certain deviation between the self-sensing characteristics during the cooling process and the linear model used, which inevitably leads to the deterioration of the estimated error. According to the data in Tables 1 and 2, it can also be seen that larger estimation errors in Case II result in a decrease in tracking performance. It should be noted that in this experiment, the abrupt changes in the desired trajectory, significant transient errors can occur during step trajectory tracking. However, the RMS value of errors is more focused on the

accuracy of the steady state. If larger transient errors are included in the calculation of the RMS value, it will overshadow more steady-state information. Therefore, when calculating e_{rms} , only data with absolute values below 0.04 mm were selected, so that e_{rms} can better reflect the steady-state characteristics.

From the data in Table 2, Fig. 12(b) and (d), it can be visually observed that after adopting self-sensing displacement feedback, compared to the case with sensor, there is a significant deterioration in tracking control performance, especially steady-state performance, even though integral control is applied. This is caused by the errors of the self-sensing model itself. However, after introducing compensation, it can be seen that the convergence rate of the error is significantly improved, and the steady-state error is also significantly reduced, especially during the cooling process of the SMA wire where the displacement decreases. At certain moments, the steady-state performance is even better than that of sensor-based control. This fully demonstrates that without improving the measurement accuracy of the self-sensing model, the control performance can also be effectively improved by the compensation method proposed in this paper.

The control results under a triangular wave trajectory with a period of 5 s and an amplitude of 0.4 mm are shown in Fig. 13. Firstly, it can be observed from Fig. 13(c) that the estimated accuracy of self-sensing is similar for the three different control methods, which is consistent with the conclusion shown in Table 1. From Fig. 13(b) and its zoomed-in region, it can be seen that Case II, after using self-sensing estimation as feedback, deviates significantly from the reference trajectory in terms of actual tracking performance, while Case I and III show much better performance in comparison. According to the tracking error curve plotted in Fig. 13(d) and the data in Table 2, it can be seen that after introducing compensation, the e_{rms} of Case III is 16.79 μm , which is only 39.2% of the uncompensated one, i.e., Case II. Although the tracking performance at the trajectory corners has not been completely compensated, resulting in no significant decrease in e_{max} , it still fully demonstrates the excellent performance of this compensation method.

Next, in Fig. 14, we present the tracking control results of a sinusoidal trajectory with a period of 20 s. Due to the smoother and slower nature of this trajectory compared to the previous two, the accuracy of all three control methods is significantly improved. From the data shown in Table 2, it can be seen that the e_{rms} of Case I and III are both around 6 μm , while e_{max} is approximately 20 μm . Considering that the displacement measurement resolution of the used magnetostrictive sensor used is only 10 μm , it can be said that the excellent control results have been achieved. Additionally, it is worth noting that the estimated error displayed in Fig. 14(c) for Case III is even larger than the tracking error shown in Fig. 14(d). It should be noted that, Due to the variable speed and acceleration characteristics of a sinusoidal trajectory, larger tracking errors are inevitable at points of direction change, especially when there is a high acceleration. This is a normal physical phenomenon. Additionally, the inherent modeling errors in the self-sensing model further exacerbate the degradation of

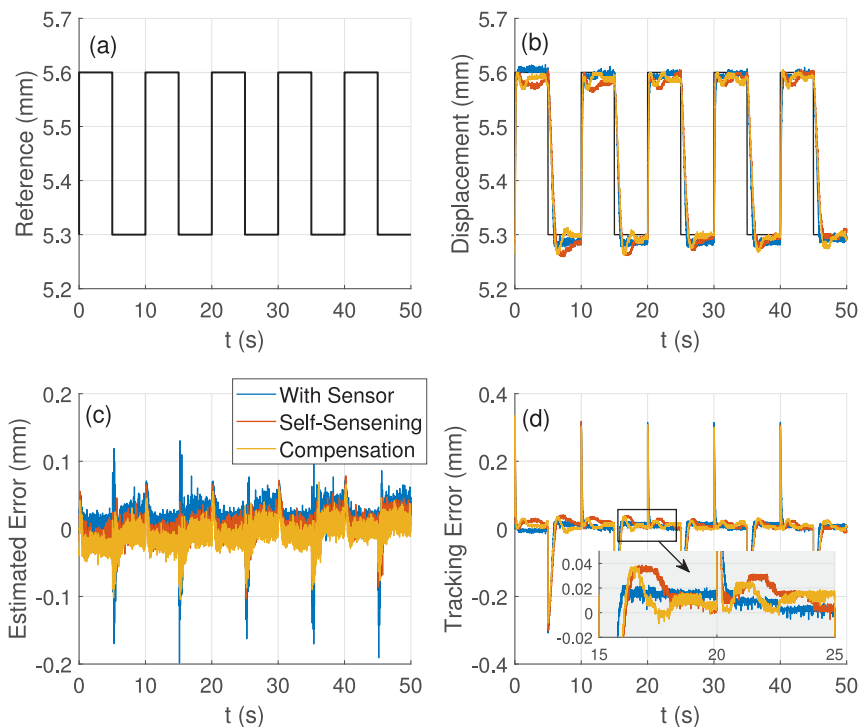


Fig. 12. Square wave trajectory: (a) Reference trajectory. (b) Actual measured displacement. (c) Estimated error. (d) Tracking error.

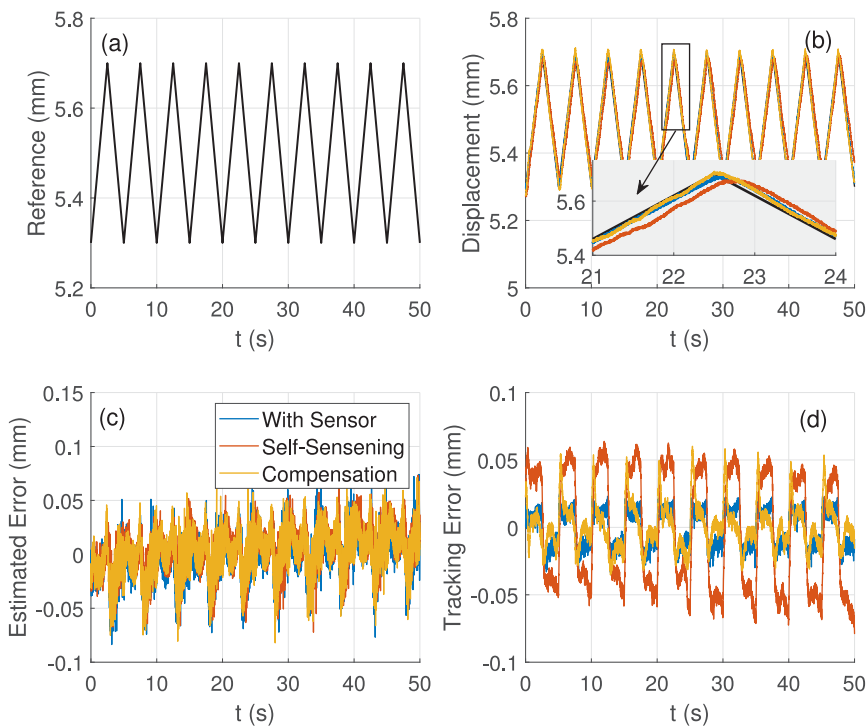


Fig. 13. Triangular wave trajectory: (a) Reference trajectory. (b) Actual measured displacement. (c) Estimated error. (d) Tracking error.

control performance. However, it should be noted that after applying the position compensation method proposed in this paper, the aforementioned errors are effectively suppressed, clearly demonstrating the effectiveness of the proposed approach. This is unimaginable for conventional methods that rely on improving the accuracy of self-sensing models to enhance trajectory tracking control performance. However,

it can be achieved through the compensation method proposed in this paper. Furthermore, the results in Fig. 14(b) and (d) show a significant improvement in the accuracy of self-sensing feedback control after compensation, which is already comparable to feedback control with sensors. This is undoubtedly good news for the implementation of control systems, demonstrating that the proposed method has the

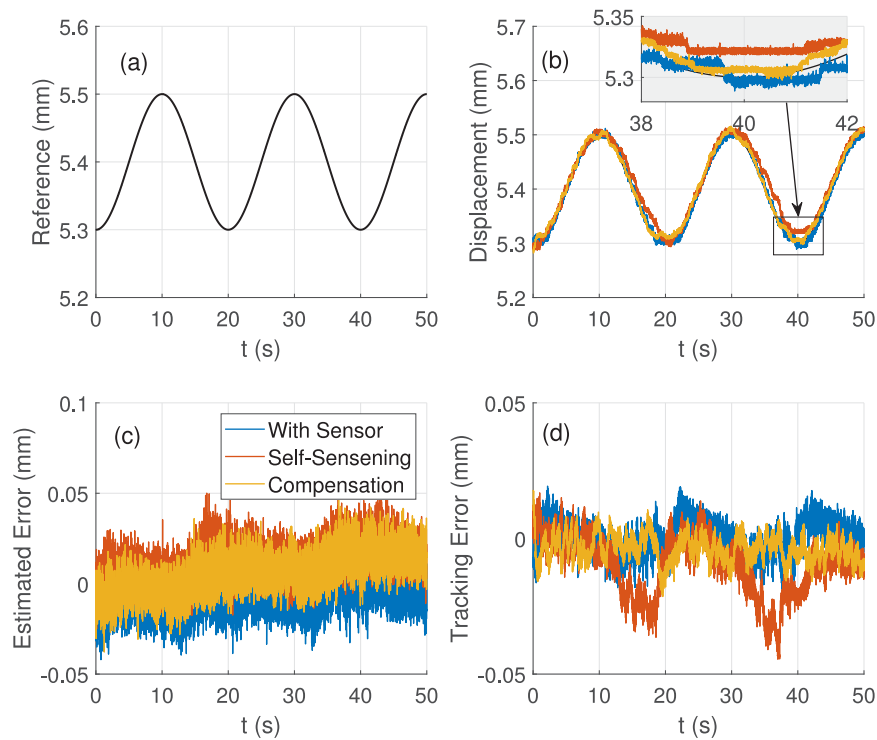


Fig. 14. Sine wave trajectory: (a) Reference trajectory. (b) Actual measured displacement. (c) Estimated error. (d) Tracking error.

potential to replace conventional displacement sensors with a simple self-sensing model in slow and smooth trajectory tracking control, and achieving more possibilities for the applications of SMA actuators.

In addition to the self-sensing characteristic testing experiments under different loads mentioned earlier, we have also performed tracking control experiments with sine wave trajectories under 30 g and 50 g loads. The experimental results are shown in Figs. 15 and 16, respectively. The tracking control errors of the three controllers under different loads are listed in Table 2. From the experimental results, it can be seen that the control performance is not significantly different after adding the load compared to before the load was added. It should be noted that even under the circumstance of adding additional load, the trajectory compensation proposed in this paper can effectively reduce tracking control errors, making the compensated tracking error close to the feedback control with position sensors. Moreover, it can be seen that despite the large modeling error of self-sensing under this condition, the tracking error can still be reduced to a relatively ideal range, which demonstrates that the compensation control method proposed in this paper can achieve excellent control performance without relying on high-precision self-sensing models.

4.3. Discussion

Regarding the above experimental results, we provide the following additional discussion:

1. Although the compensation method used in this study utilizes measured values from sensors, it does not mean that real-time measurements from sensors are required to complete the compensation. Instead, for the same type of control task, the real error is measured in advance by the sensor, and then this error sequence is offline fixed to calculate the compensation term. In the real-time control of Case III mentioned above, only the estimated displacement based on the self-sensing characteristics of SMA is used as feedback without the assistance of additional sensors. The additional sensors are only used to validate the synchronized measurement results.

2. The trajectory compensation process described above is essentially an iterative optimization process. This paper introduces the concept and presents a simple implementation. For further improvement in accuracy, multiple iterations similar to iterative learning control can be implemented.
3. The deformation of the SMA wire is directly related to its length. Due to the high integration requirements of the designed prototype, relatively short SMA wire is used, which limits the move range of the actuator itself. In future research, we will propose solutions to achieve longer move ranges to further expand the application scope of the actuator.

We agree that a nonlinear hysteresis self-sensing model considering the delay effect may achieve higher self-sensing accuracy than the existing methods proposed in this paper. However, according to the literature, the following issues exist when using the self-sensing model considering hysteresis in practice:

1. The modeling process is complex and the model solving difficulty is high. The nonlinear hysteresis component is not conducive to a real-time displacement solution for self-sensing control.
2. The nonlinear phase transition process of SMA wire is related to many factors such as current drop rate and load. Some of the reported studies cannot accurately provide a nonlinear hysteresis model that includes all influencing factors. Moreover, the size of the load cannot be accurately determined in practical applications, resulting in poor applicability of the model.
3. Due to the small displacement of the actuator in this paper, the impact of nonlinear hysteresis is not significant. The compensation method proposed in this paper can meet the requirements of motion accuracy. Furthermore, its implementation method is simple without complicated modeling process. Therefore, we did not specifically conduct nonlinear hysteresis modeling in our research.

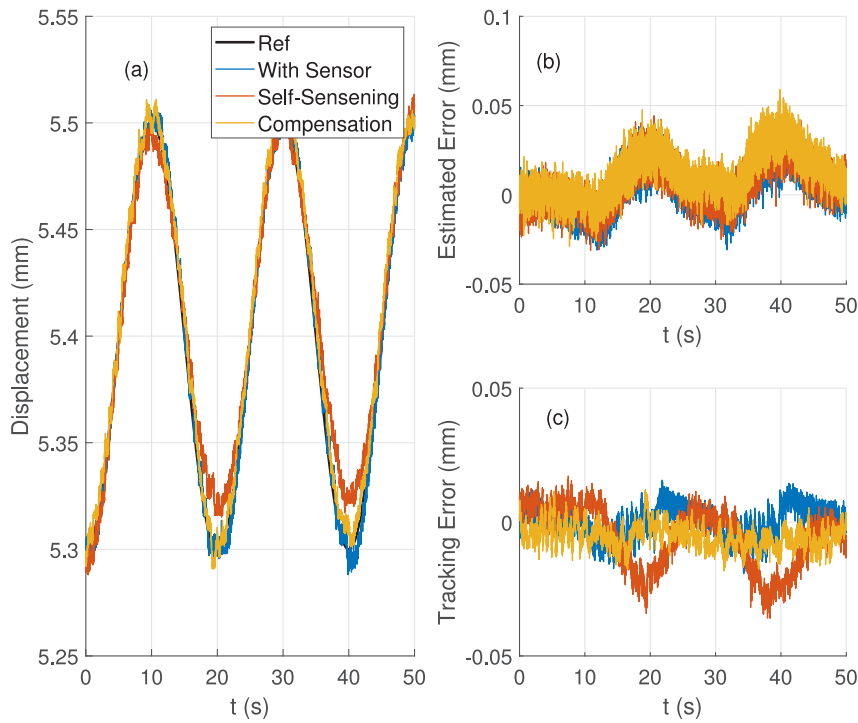


Fig. 15. Sine wave trajectory with 30 g load: (a) Reference trajectory and actual measured displacement. (b) Estimated error. (c) Tracking error.

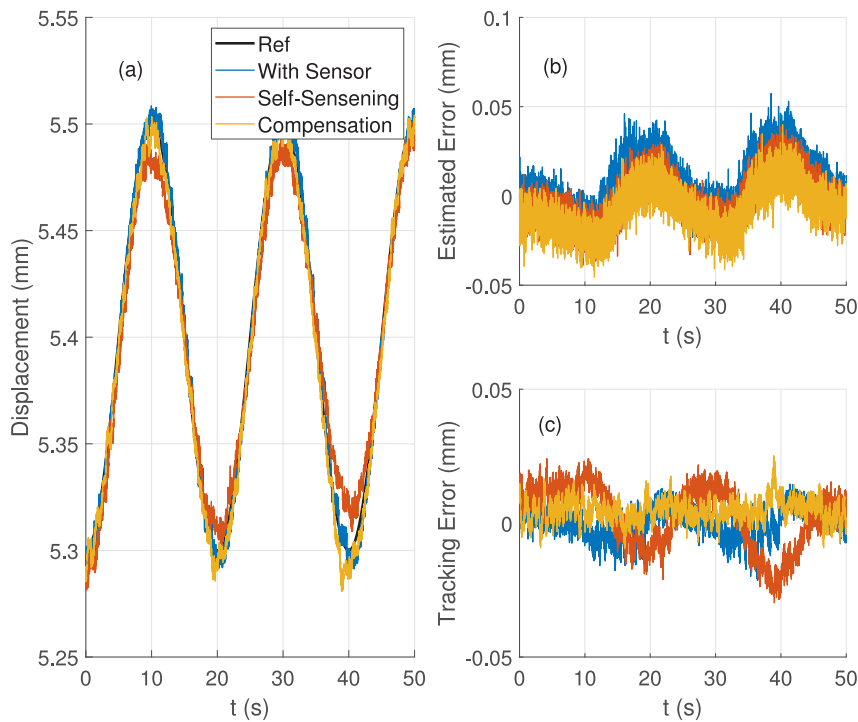


Fig. 16. Sine wave trajectory with 50 g load: (a) Reference trajectory and actual measured displacement. (b) Estimated error. (c) Tracking error.

5. Conclusion

In this paper, a highly integrated prototype of SMA actuator is designed, where the auxiliary position sensor and self-resetting spring are highly integrated, achieving a more compact size compared to existing SMA actuators. Furthermore, addressing the contradiction between model accuracy and complexity in SMA self-sensing characteristics, which affects the effectiveness of self-sensing control, a novel self-sensing control and compensation method is proposed. Firstly, a

preliminary self-sensing model is established based on test results and approximated using the simplest linear model. Then, the less accurate position estimation is directly used as feedback for the control system, and the tracking error is directly compensated to enhance control performance. A series of tracking control experiments are conducted, and the results demonstrate that the proposed method achieves accurate tracking control even in the presence of significant errors in the self-sensing model. The integrated prototype and the precision enhancement strategy without additional position sensors presented

in this paper provide more possibilities for downsized and real-time applications of SMA actuators.

Declaration of competing interest

The authors declare the following financial interests/personal relationships which may be considered as potential competing interests: Ze Wang reports financial support was provided by National Natural Science Foundation of China, Beijing Natural Science Foundation and CIE-Tencent Robotics X Rhino-Bird Focused Research Program.

Data availability

The data that has been used is confidential.

Acknowledgment

This work is supported by National Natural Science Foundation of China under Grant 52205532, Beijing Natural Science Foundation under Grant 3242005, and CIE-Tencent Robotics X Rhino-Bird Focused Research Program.

References

- [1] Ze Wang, Chuxiong Hu, Yu Zhu, Accelerated iteration algorithm based contouring error estimation for multi-axis motion control, *IEEE/ASME Trans. Mechatronics* 27 (1) (2021) 452–462.
- [2] Ze Wang, Chuxiong Hu, Yu Zhu, Ming Zhang, Chi Zhang, The modular design of trajectory compensation based on ATCF for precision motion control, *Mech. Syst. Signal Process.* 135 (2020) 106393.
- [3] Ze Wang, Chuxiong Hu, Yu Zhu, Suqin He, Kaiming Yang, Ming Zhang, Neural network learning adaptive robust control of an industrial linear motor-driven stage with disturbance rejection ability, *IEEE Trans. Ind. Inform.* 13 (5) (2017) 2172–2183.
- [4] Ze Wang, Ran Zhou, Chuxiong Hu, Yu Zhu, Online iterative learning compensation method based on model prediction for trajectory tracking control systems, *IEEE Trans. Ind. Inform.* 18 (1) (2022) 415–425.
- [5] Jin Yang, Chuxiong Hu, Yu Zhu, Ze Wang, Ming Zhang, Experimental investigation of shaping disturbance observer design for motion control of precision mechatronic stages with resonances, *Mechanical Systems and Signal Processing* 92 (2017) 334–348.
- [6] Junfeng Li, Position control based on the estimated bending force in a soft robot with tunable stiffness, *Mech. Syst. Signal Process.* 134 (2019) 106335.
- [7] Yong Zhong, Ruxu Du, Peng Guo, Haoyong Yu, Investigation on a new approach for designing articulated soft robots with discrete variable stiffness, *IEEE/ASME Trans. Mechatronics* 26 (2021) 2998–3009.
- [8] Xiaonan Huang, Michael Ford, Zach J. Patterson, Masoud Zarepoor, Chengfeng Pan, Carmel Majidi, Shape memory materials for electrically-powered soft machines, *J. Mater. Chem. B* 8 (2020) 4539–4551.
- [9] Lorenza Petrini, Francesco Migliavacca, Biomedical applications of shape memory alloys, *J. Metall.* 2011 (2011) 1–15.
- [10] Jung Sohn, Gi-Woo Kim, Seung-Bok Choi, A state-of-the-art review on robots and medical devices using smart fluids and shape memory alloys, *Appl. Sci.* 8 (2018) 1928.
- [11] Andrea Sellitto, Aniello Riccio, Overview and future advanced engineering applications for morphing surfaces by shape memory alloy materials, *Materials* 12 (2019) 708.
- [12] Krishna Chaitanya S., Dhanalakshmi K., Demonstration of self-sensing in Shape Memory Alloy actuated gripper, 2013.
- [13] Yifan Lu, Zhijie Xie, Jian Wang, Honghao Yue, Miao Wu, Yiwei Liu, A novel design of a parallel gripper actuated by a large-stroke shape memory alloy actuator, *Int. J. Mech. Sci.* 159 (2019) 74–80.
- [14] Hu Jin, Yiming Ouyang, Haoyao Chen, Jingwen Kong, Weihua Li, Shiwu Zhang, Modeling and motion control of a soft SMA planar actuator, *IEEE/ASME Trans. Mechatronics* 27 (2022) 916–927.
- [15] R. Rusinek, J. Warminski, M. Szymanski, K. Kecik, K. Kozik, Dynamics of the middle ear ossicles with an SMA prosthesis, *Int. J. Mech. Sci.* 127 (2017) 163–175.
- [16] Ning An, Meie Li, Jinxiong Zhou, Modeling SMA-enabled soft deployable structures for kirigami/origami reflectors, *Int. J. Mech. Sci.* 180 (2020) 105753.
- [17] Jing-Han Guan, Yong-Chen Pei, Ji-Tuo Wu, A driving strategy of shape memory alloy wires with electric resistance modeled by logistic function for power consumption reduction, *Mech. Syst. Signal Process.* 160 (2021) 107839.
- [18] Michele A. Mandolino, Dominik Scholtes, Francesco Ferrante, Gianluca Rizzello, A physics-based hybrid dynamical model of hysteresis in polycrystalline shape memory alloy wire transducers, *IEEE/ASME Trans. Mechatronics* (2023) 1–12.
- [19] Byeongkyu Lim, Changhun Lee, Donghyun Hwang, Development of embedded sensor system for 5-DOF finger-wearable tactile interface, *IEEE/ASME Trans. Mechatronics* 26 (2021) 1728–1736.
- [20] Chen Zhang, Yewei Yu, Jingwen Xu, Miao Zhou, Hysteresis modeling and analysis of magnetic shape memory alloy-driven actuator, *IEEE Trans. Nanotechnol.* 21 (2022) 390–398.
- [21] Jaeyeon Jeong, Kyujin Hyeon, Jungwoo Han, Cheol Hoon Park, So-Young Ahn, Soo-Kyung Bok, Ki-Uk Kyung, Wrist assisting soft wearable robot with stretchable coolant vessel integrated SMA muscle, *IEEE/ASME Trans. Mechatronics* 27 (2022) 1046–1058.
- [22] Qingpeng Ding, Jianghua Chen, Wanquan Yan, Kim Yan, Andre Kyme, Shing Shin Cheng, A high-performance modular SMA actuator with fast heating and active cooling for medical robotics, *IEEE/ASME Trans. Mechatronics* 27 (2022) 5902–5913.
- [23] Josephine Selvarani Ruth D, Sunjai Nakshatharan S, Dhanalakshmi K, Differential resistance feedback control of a self-sensing shape memory alloy actuated system, *ISA Trans.* 53 (2014) 289–297.
- [24] Josephine Selvarani Ruth D., Dhanalakshmi K., Shape memory alloy wire for self-sensing servo actuation, *Mech. Syst. Signal Process.* 83 (2017) 36–52.
- [25] Fengqiang Bai, Xiangjun Zhang, Dianguo Xu, Accurate position tracking control of SMAAs based on low-complexity self-sensing model and compound control strategy, *IEEE Sens. J.* 23 (2023) 2280–2290.
- [26] Jing-Han Guan, Yong-Chen Pei, Ji-Tuo Wu, Bao-Hua Wang, Wen-Chao Sui, Sheng-Run Li, A self-sensing and robust resistance phase transition detection method for the displacement estimation of shape memory alloy wires, *Mech. Syst. Signal Process.* 170 (2022) 108862.
- [27] Junfeng Li, Huifang Tian, Position control of SMA actuator based on inverse empirical model and SMC-RBF compensation, *Mech. Syst. Signal Process.* 108 (2018) 203–215.
- [28] Hari Narayan Bhargaw, Samarth Singh, B.A. Botre, S.A. Akbar, R. Hashmi, Poonam Sinha, Deep neural network-based physics-inspired model of self-sensing displacement estimation for antagonistic shape memory alloy actuator, *IEEE Sens. J.* 22 (2022) 3254–3262.
- [29] Yong-Chen Pei, Baohua Wang, Ji-Tuo Wu, Chenyang Wang, Jing-Han Guan, Huiqi Lu, A machine learning empowered shape memory alloy gripper with displacement-force-stiffness self-sensing, *IEEE Trans. Ind. Electron.* 70 (2023) 10385–10395.
- [30] Sang-Hak Lee, Sang-Woo Kim, Improved position control of shape memory alloy actuator using the self-sensing model, *Sensors Actuators A* 297 (2019) 111529.
- [31] Chao-Chieh Lan, Chen-Hsien Fan, An accurate self-sensing method for the control of shape memory alloy actuated flexures, *Sensors Actuators A* 163 (1) (2010) 323–332.

Ze Wang received the B.S. degree in automation from the School of Electricity Engineering and Automation, Tianjin University, Tianjin, China, in 2015, and the Ph.D. degree in mechanical engineering from the Department of Mechanical Engineering, Tsinghua University, Beijing, China, in 2020. He is currently an assistant professor with the Department of Mechanical Engineering, Tsinghua University. His research interests include precision motion control, neural network adaptive control, and high-performance multi-axis contouring control.

Dr. Wang was the recipient of the Best Student Paper Finalist at the 2017 IEEE/ASME International Conference on Advanced Intelligent Mechatronics, the 2017 Best Student Paper from the IEEE Internal Conference on Information and Automation, and 2019 Top Grade Scholarship for Graduate Students of Tsinghua University.

Zihang Shang is currently pursuing a Bachelor's degree in Engineering at Lappeenranta-Lahti University of Technology (LUT), Finland. Currently, he is conducting cooperative research internship work at Tsinghua University, with a primary research interest in the design and control methods of novel actuators.

Chuxiong Hu received his B.S. and Ph.D. degrees in Mechatronic Control Engineering from Zhejiang University, Hangzhou, China, in 2005 and 2010, respectively. He is currently an Associate Professor (tenured) at Department of Mechanical Engineering, Tsinghua University, Beijing, China. From 2007 to 2008, he was a Visiting Scholar in mechanical engineering with Purdue University, West Lafayette, USA. In 2018, he was a Visiting Scholar in mechanical engineering with University of California, Berkeley, CA, USA. His research interests include precision motion control, high-performance multi-axis contouring control, precision mechatronic systems, intelligent learning, adaptive robust control, neural networks, iterative learning control, and robot.

Yu Zhu received the B.S. degree in radio electronics from Beijing Normal University, Beijing, China, in 1983, and the M.S. degree in computer applications and the Ph.D. degree in mechanical design and theory from the China University of Mining and Technology, Beijing, in 1993 and 2001, respectively. He is currently a Professor with the State Key Laboratory of Tribology, Department of Mechanical Engineering, Tsinghua University, China. He has authored or coauthored more than 180 technical papers. He is also the holder of more than 140 warranted invention patents. His research interests include precision measurement and motion control, ultraprecision mechanical design and manufacturing, two-photon microfabrication, and electronics manufacturing technology and equipment.